Machine Vision and Applications manuscript No.
(will be inserted by the editor)

Antonio Fernández · Ovidiu Ghita · Elena González · Francesco Bianconi · Paul F. Whelan

Evaluation of robustness against rotation of LBP, CCR and ILBP features in granite texture classification

Received: date / Accepted: date

Abstract The aim of this paper is to conduct a performance evaluation where several texture descriptors such as Local Binary Patterns (LBP), Coordinated Clusters Representation (CCR) and (Improved Local Binary Patterns) ILBP are applied for granite texture classification. In our work we were particularly interested to assess the robustness of the analysed texture descriptors to image rotation when they were implemented in both the standard and rotation invariant forms. In order to attain this goal, we have generated a database of granite textures that were rotated using hardware and software procedures. The experimental data indicates that the ILBP features return improved performance when compared to those achieved by the LBP and CCR descriptors. Another important finding resulting from this investigation reveals that the classification results obtained when the texture analysis techniques were applied to granite image data rotated by software procedures are inconsistent with those achieved when the hardware rotated data is used for classification purposes. This discovery is surprising and suggests that the results obtained when the texture analysis techniques are evaluated on synthetically rotated data need to be interpreted with care, as the principal characteristics of the texture are altered by the data interpolation that is applied during the image rotation process.

Keywords Texture classification · Rotation invariance · LBP · CCR · ILBP · Granite grading

A. Fernández (✉) · E. González
Department of Engineering Design, Universidade de Vigo
School of Industrial Engineering, Campus Universitario, 36310 Vigo, Spain
Tel.: +34-986-818602
Fax: +34-986-812201
E-mail: {antfdez,elena}@uvigo.es

O. Ghita · P.F. Whelan
Vision Systems Group, Dublin City University
School of Electronic Engineering, Dublin City University, Glasnevin, Dublin 9, Ireland
E-mail: ghitao@eeng.dcu.ie, paul.whelan@dcu.ie

F. Bianconi
Department of Industrial Engineering, Università degli Studi di Perugia
Via G. Duranti 67, 06125 Perugia, Italy
E-mail: bianco@unipg.it

1 Introduction

Texture analysis is an area of active research in machine vision. Five canonical problems related to texture analysis are segmentation, classification, synthesis, shape from texture and image retrieval. Texture classification techniques find one of their most important industrial applications in grading products according to their visual appearance. In many industrial sectors, e.g. paper [47], ceramic tiles [18], wood [45], leather [15], marble [32], fabric [3], painted slates [13], etc., there is a growing interest in systems that perform this task automatically. In recent years, great effort has been put into developing laboratory prototypes. However, to the best of our knowledge, commercial systems suitable to grade these products in an industrial environment are not yet available.

Granite industry is also concerned in the development of an automated machine vision system for sorting granite plates in lots that exhibit similar visual characteristics. Due to its combination of strength, beauty and affordable price, granite has become increasingly popular in façade cladding and pavement covering. The price of granite, just like other ornamental materials, is mainly determined by its aesthetical value (i.e. visual appearance) rather than its mechanical properties. There is a wide range of commercially available granite varieties, with different predominant colours (green, pink, black, red, etc.) and textures (veined, speckled, homogeneous, etc.). Existing standards for granite inspection focus on geometrical specifications, such as longitudinal dimensions of blocks, flatness of slabs or straightness of tile

edges. However, the specification of visual appearance is imprecise [44]. Granites have been usually designated by a generic name beside the predominant colour, for example "Baltic Brown", "Emerald Pearl" or "Imperial Pink". It should be pointed out that this terminology varies from one country to another. Globalization has increased the need for a standard denomination of granites. The solution adopted is to give a product name and to specify the place of origin for any particular rock, in addition to the traditional name and typical colour [12]. This nomenclature is useful when viewed from a commercial perspective, but is not so relevant in the process of grading automatically the granite plates. The problem is not solved by using more sophisticated petrographical descriptions, because the visual appearance of granites with the same mineralogical nature may differ significantly. The lack of precision in the specification of visual appearance often leads to controversial situations between customers and suppliers. In many cases, the customer refuses a lot of granite plates arguing that it does not resemble the sample that served as basis for the purchase. Another frequent source of complaint is the lack of uniformity in the visual appearance of the plates that make up the lot. As a result of these conflicts, granite companies can incur heavy losses due to, on the one hand, costly shipping charges, and on the other hand, penalties established in the contract to compensate for delays in building works owing to late delivery. In order to overcome these issues, granite industry has implemented quality control procedures, consisting of a visual inspection performed by a skilled operator. Although this qualitative assessment prevents lot rejection to a great extent, it is not a satisfactory solution because the decisions made by the human operator are subjective (being highly biased by the experience of the skilled operator) and non-repetitive.

A number of papers on automatic classification of granite textures have been published in the last few years. Former approaches to granite texture modeling were based on colour features, such as colour histogram [46] or chromaticity moments [38]. Later, better results were obtained through gray-scale texture classification approaches, such as co-occurrence matrices [37,36], Gabor filter banks [24,4] and Coordinated Clusters Representation (CCR) [20,42,14]. This is motivated by the fact that the granite plates are defined by strong crystalline structures while the color information is less pronounced. Most recently, classification accuracy has been further improved by considering colour and texture features jointly [22,7]. In all these works the granite images were recorded under controlled environmental conditions. Achieved recognition rate ranges from ≈70% to 100%. This spread in the classification accuracy may be partly explained by the different performance of the features and classifiers used, and the intrinsic difficulty of the dataset, but it is useful to note that factors related to the image acquisition procedure may have an important effect on the classification results. Additional factors that may effect on the classification accuracy include parameters such as image size, noise, quantization level and the degree of similarity between granite textures. Furthermore, the lowest values of misclassification rate were obtained when the train and test images were overlapped subimages of a texture image. This is a frequent solution when few texture images are available to train the classifier. However, using overlapped texture images invariably leads to underestimation of the generalization error. Nowadays, there is a trend in the granite texture classification research community of pooling the output of several classifiers designed in different feature spaces [25–27] in order to attain increased ensemble success rate.

Sensitivity to rotation is a major issue in certain applications of texture classification. The overall performance of a texture classifier may be totally degraded if the unknown patterns to be classified are slightly rotated with respect to the training samples. Provided that real-world textures can occur at any orientation, a large emphasis has been put in the development of rotation invariant texture descriptors. Rotation invariance has been often accomplished by modifying well-known non invariant approaches, such as wavelets, Markov random fields and Gabor filtering [39]. The same happened in the case of local binary patterns (LBP), which were first defined for a 3×3 pixels squared neighbourhood, and were later generalized for circular domains [34] to remove sensitivity to rotation.

The main goal of this paper is to evaluate LBP, CCR and ILBP features when applied to the classification of granite images in order to determine which descriptor is most effective. The reason why we chose this family of texture descriptors among the vast plethora of features currently available is multiple-fold. First, these techniques offer an excellent approach to analyse the texture at micro level by analysing the distribution of the local texture elements (i.e. local binary patterns) and in addition they entail a low computational overhead, a fact that makes them attractive when applied in the implementation of real-time industrial applications. Thus, by using these techniques one could achieve real-time processing in a manufacturing plant, since current hardware allows feature extraction from granite plates at a higher rate than the operational speed of the conveyor. Second, the local binary pattern related techniques are parameter-free and as a result they do not require complex optimisation procedures, as many other methods do. Third, the LBP, CCR and ILBP texture descriptors are intrinsically invariant to changes in illumination intensity and monotonic image transforms. Fourth, these features have been proven to be effective and accurate in discriminating texture. Due to the advantageous characteristics just mentioned, the binary pattern is a well-known approach to texture analysis (with the main focus being placed on the LBP model) and it has received substantial interest from image analysis practitioners. In this

study, we evaluate two different approaches to achieve rotation invariance: grouping circularly symmetric patterns and computing the DFT of features. These methods were applied to all the features considered. In our experiments we employed one database of granite texture images recorded in the lab by means of a portable acquisition system, formed by a still camera and a special illumination set-up. To quantitatively assess the robustness against rotation of LBP, CCR and ILBP we have performed classification trials for different relative orientations of the test samples with respect to training samples. Our results confirmed previous findings on these texture descriptors [33,41,7] by showing that: (a) their basic versions are very efficient in recognizing unrotated textures and, (b) the rotation invariant versions are, to a great extent, robust against rotation. However, we surprisingly found that the performance of the supposed rotation invariant versions of LBP, CCR and ILBP strongly depends on the method through which the rotated textures are obtained (either hardware or software). We also found that the degree of immunity against rotation also depends on the methods employed to make features rotation invariant.

The remainder of the paper is organized as follows: LBP, CCR and ILBP features are reviewed in Section 2. The methods for achieving rotation invariance are explained in Section 3. The prototype for granite image acquisition is described in Section 4. Quantitative assessment of sensitivity to rotation of the considered texture descriptors is presented in Section 5, and Section 6 concludes the paper.

2 LBP and CCR texture models

A key issue in texture classification is the choice of a suitable model to represent texture. There exists a great number of approaches, which are commonly divided in four categories: statistical, structural, model-based and signal processing methods [50]. Statistical approaches describe the texture in terms of the spatial distribution of the pixel intensities, while structural methods regard the texture as the hierarchical distribution of certain image primitives. LBP, CCR and ILBP are closely related texture descriptors that lie between both approaches. In fact, LBP has been proposed as the *unifying approach* to the traditionally divergent statistical and structural methods [31].

LBP, CCR and ILBP are inspired in the texture spectrum approach, which exploits the occurrence of certain elementary patterns, called texture units [48]. A texture unit is defined by the local distribution of the intensities of adjacent pixels in a 3×3 neighbourhood, each of which can take three possible values. All these features may be considered two-level particularizations of the texture spectrum. The underlying idea is that a texture can be represented through a histogram which quantifies how frequently binary patterns appear in it. The remainder of this section is devoted to describe these texture models in their basic versions.

2.1 LBP

The basic version of the LBP texture operator, denoted by $\mathrm{LBP}_{3\times3}$, works with the eight neighbours of a pixel, using the gray level of the central pixel as a binarization threshold. To produce a $\mathrm{LBP}_{3\times3}$ code for a neighbourhood, binary values are weighted with different powers of two, and the result is summed up [31]. Since the binary pattern is formed by 8 bits, there are 2^8 different binary patterns, and hence, the $\mathrm{LBP}_{3\times3}$ histogram has 256 bins (Fig. 1(a)). A number of extensions to the basic LBP operator have been developed [34]: (a) rotation invariant, (b) multiple resolutions and, (c) contrast complementary measure. In this paper we focus on rotation invariance.

2.2 CCR

The CCR texture descriptor was first proposed by Kurmyshev and Cervantes [19]. This model, which was originally intended for binary textures, relies on the histogram of occurrence of the elemental patterns of binary texture, called *texels*, that can be defined in a square window. The dimension of these elementary patterns is usually set to 3×3 pixels, since this size provides good discriminative power at a reasonable cost in terms of both computational speed and memory usage.

The CCR model was later applied to gray-scale texture images through global image thresholding. A thorough literature review revealed that very similar approaches were proposed almost at the same time by different authors who worked independently. A research group from Krasnoyarsk State Technical University, Russia, presented in 2002 a technique for the analysis of anisotropy of digital images that, when particularized to binary images, closely resembles the CCR concept [17]. In this case, the key elements of their method, namely *frequency mosaic* and *smalts*, play the role of CCR histogram and texels, respectively. The natural extension of the former CCR features to gray-scale texture classification was reported in 2003 by a group from the Center for Research on Optics, Mexico [41,42]. In the same year, a group from the Yuan-Ze University, Taiwan, proposed the local edge pattern (LEP) texture model [51]. The basic idea is to obtain an edge image by applying the Sobel edge detector to the intensity channel of colour images, and then to binarize the edge image by using a heuristic threshold (150 in their implementation). The spatial structure of the resulting binary image is described by the histogram of LEP patterns, which are actually the texels of the CCR model.

In principle, thresholding can cause significant loss of information in the original image and, as a consequence,

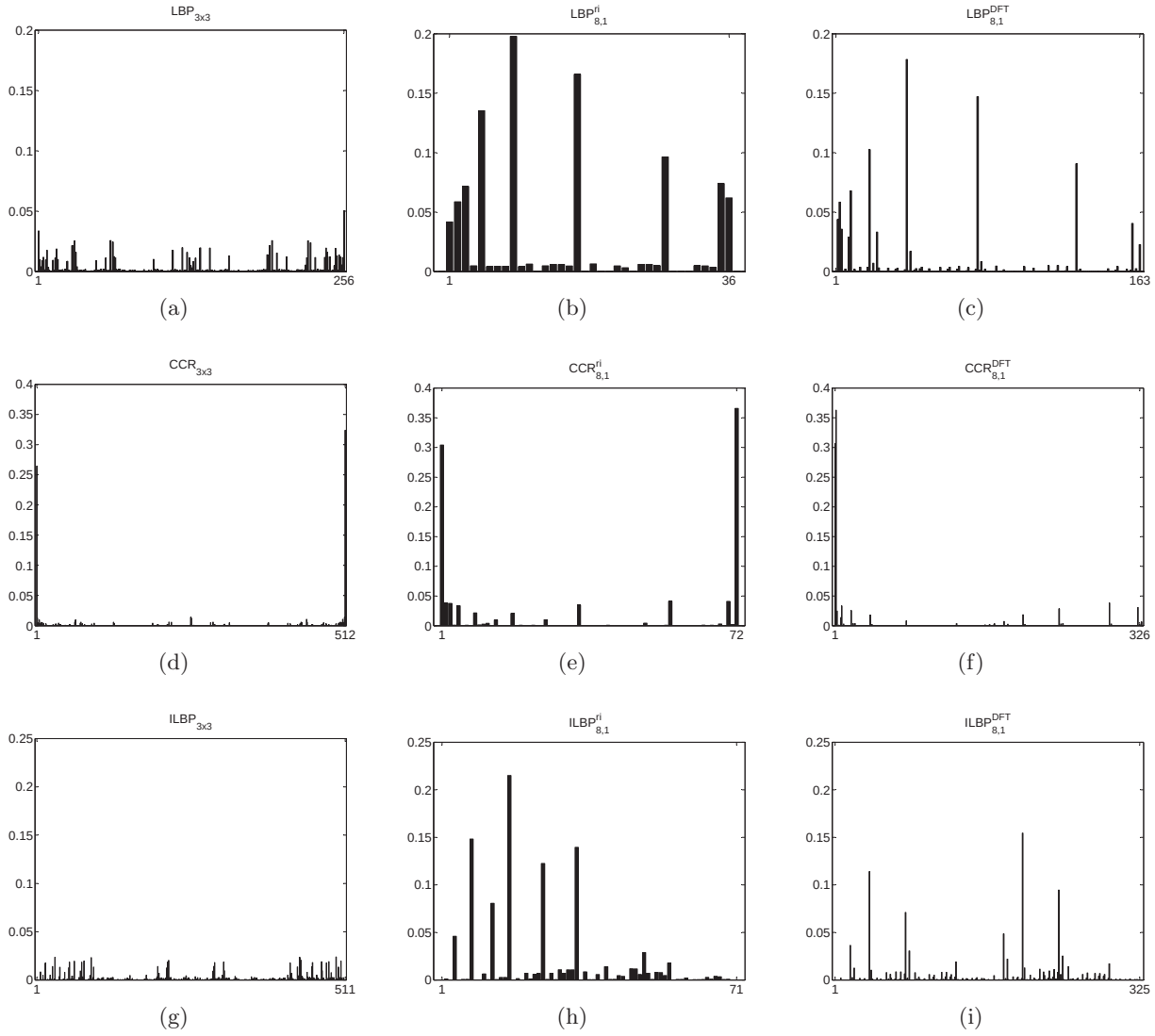

Fig. 1 Feature histograms corresponding to the granite texture *Azul Platino* (Fig. 5), obtained with the following operators: **(a)** $\mathrm{LBP}_{3\times3}$, **(b)** $\mathrm{LBP}^{ri}_{8,1}$, **(c)** $\mathrm{LBP}^{DFT}_{8,1}$, **(d)** $\mathrm{CCR}_{3\times3}$, **(e)** $\mathrm{CCR}^{ri}_{8,1}$, **(f)** $\mathrm{CCR}^{DFT}_{8,1}$, **(g)** $\mathrm{ILBP}_{3\times3}$, **(h)** $\mathrm{ILBP}^{ri}_{8,1}$ and **(i)** $\mathrm{ILBP}^{DFT}_{8,1}$.

some textures could become indistinguishable. Threshold should be judiciously chosen in order to preserve textural information. A great variety of image thresholding techniques have been proposed in literature [43]. So far, two thresholding methods have been applied to CCR, namely fuzzy C-means clustering [41] and isoentropic partition [5]. A major drawback of the fuzzy C-means algorithm is its intrinsic randomness. This means that different executions could yield different thresholds for the same image. To avoid this issue, in this work we used the isoentropic quantization approach. Briefly, in this method the binarization threshold is the gray level which splits the entropy of the gray-level histogram of an image into two equal parts.

The procedure to assign a $\mathrm{CCR}_{3\times3}$ code to a texel is analogous to the $\mathrm{LBP}_{3\times3}$ case. The main difference with respect to $\mathrm{LBP}_{3\times3}$ is that the threshold used to binarize the texture image is global rather than local. Consequently, texels are formed by 9 bits, and therefore the $\mathrm{CCR}_{3\times3}$ histogram has 2^9=512 bins (Fig. 1(d)).

2.3 ILBP

The ILBP (Improved Local Binary Patterns) [16] can be considered a hybrid between the CCR and the LBP: on the one hand, the ILBP resembles the CCR model in that all the pixels of the 3×3 window are used (while in the case of the LBP the central pixel is discarded); on the other hand, the ILBP resembles the LBP in that local thresholding is used (while in the case of the CCR thresholding is global). The local threshold is computed

by averaging the gray-level values of the 3×3 neighbouring pixels. The number of different ILBP patterns is $2^9 - 1 = 511$, since, by definition, it is impossible that all the pixels of the neighbourhood are lower than the average value.

2.4 Considerations about LBP, CCR and ILBP

The above described models characterize texture by means of a histogram which quantifies the relative occurrence of certain binary patterns. The only difference is that LBP and ILBP use a local binarization threshold, while CCR uses a global one. Strictly speaking the LBP and ILBP are models to characterize gray-scale textures, whereas the CCR model is intended to describe binary textures. Thus, when the CCR approach is applied to gray-scale textures, a pre-processing step that involves the binarisation of the input image has to be applied prior to the calculation of the binary texture units.

Let's now consider a finely defined texture, like those shown in Fig. 5. There is a high probability that all the pixels of a 3×3 neighbourhood have gray levels below or above a global threshold. In contrast, the probability that all the outer pixels have gray levels below or above the gray level of the central pixel is quite low. Accordingly, the relative frequency of the binary patterns formed by all 0's or 1's (from now on these patterns will be referred to as *constant* patterns) is low when the $\mathrm{LBP}_{3\times3}$ operator is used, while in the $\mathrm{CCR}_{3\times3}$ model these patterns are the majority. Regarding the ILBP constant patterns, the one formed by all 1's is very unlikely, while the one formed by all 0's cannot occur at all by definition. Such considerations explain why the $\mathrm{CCR}_{3\times3}$ histograms present two pronounced peaks located at bins 1 and 512 (of Fig. 1(d)), which correspond to completely black texels and completely white texels, respectively. These peaks are less pronounced in the case of the LBP (Fig. 1(a))) and vanish in the case of the ILBP (Fig. 1(g))). It should be noticed that in Figs. 1(a)-1(i) the histogram bins have been labeled using correlative numbers from 1 to the dimension of the feature space, rather than assigning a bin to the decimal code representative of the corresponding binary pattern.

The last point worth discussing is the theoretical foundation of these texture models. The aptitude of the LBP and ILBP models to characterize gray-scale textures relies solely on the excellent results obtained in texture classification experiments. In contrast, the effectiveness of the CCR model in discriminating binary textures is supported by certain underlying statistical principles. The fundamental properties of $\mathrm{CCR}_{3\times3}$ features were stated in two theorems [19]: the first theorem establishes the structure of the CCR of periodic binary images, and the second one establishes the relation between the CCR histogram and the correlation moments of n-th order of a binary image. It is widely recognized that the second and higher order joint probability density functions provide structural information about a gray-scale texture. If the gray-scale texture to be classified is thresholded in a way that keeps sufficiently enough structural information, the arguments above demonstrate that the CCR model is highly suitable for recognition and classification of gray-scale texture images.

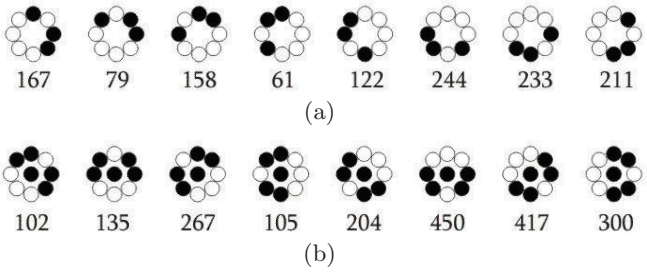

Fig. 2 Rotated versions of a binary pattern, which are merged in the same bin of the **(a)** $\mathrm{LBP}^{ri}_{8,1}$ and **(b)** $\mathrm{CCR}^{ri}_{8,1}$ histograms. Pattern codes are indicated underneath.

3 Rotation invariance

We considered two approaches to obtain rotation invariant versions of the above described texture models. The first one is based on rotation invariant patterns, the second one uses the Discrete Fourier Transform. The two methods are described in the following subsections. The first step of both methods consists in replacing the original 3×3 window by a circular one. The values of neighbours that do not lie exactly on the original pixels positions are estimated through bilinear interpolation [34]. The resulting feature spaces are referred to as $\mathrm{LBP}_{8,1}$, $\mathrm{ILBP}_{8,1}$, and $\mathrm{CCR}_{8,1}$.

3.1 Rotation invariant patterns

The rotation invariant LBP operator, denoted by $\mathrm{LBP}^{ri}_{8,1}$, is straightforwardly achieved by considering that the different patterns obtained by rotating a particular pattern in 45^{o} steps are actually the same pattern, and therefore they can be grouped together [34]. In this manner, the descriptor becomes more compact since the number of bins of the histogram reduces to 36 (Fig. 1(b)). This situation is illustrated in Fig. 2(a) for the pattern coded 167. This pattern and its rotated versions (namely 61, 79, 122, 158, 211, 233 and 244) are merged in bin number 26 of the $\mathrm{LBP}^{ri}_{8,1}$ histogram. The constant patterns, those binary patterns in which all the pixels take the same value 0 or 1 (e.g. patterns 0 and 255) remain the same when rotated. Rotation invariance of CCR and ILBP features can be obtained in a similar way [7]. In these cases the resulting number of bins of the histogram is 72 and 71 (Figs. 1(e) and 1(h)), respectively . An example is shown

in Fig. 2(b), where the pattern coded 102 is represented together with its rotated versions (namely 105, 135, 204, 267, 300, 417 and 450). These eight patterns are merged in the bin with the index 35 of the $\mathrm{CCR}^{ri}_{8,1}$ and $\mathrm{ILBP}^{ri}_{8,1}$ histograms.

It is useful to notice that the rotation invariant patterns may be approached from the standpoint of abstract algebra. Indeed, an important result from combinatorial group theory, the Cauchy-Frobenius lemma [49], is a suitable tool to determine in a formal fashion the number of groups of rotationally equivalent patterns. For the sake of simplicity we will use instead a more concise statement, known as the Burnside theorem [2]. Let G be a permutation group (in this context the term *group* denotes an algebraic structure) that acts on a set S. The theorem says that the number of equivalence classes into which S is divided by the equivalence relation induced by G is given by:

$$\#\{S/G\} = \frac{1}{\#\{G\}} \sum_{\pi \in G} \#\{S_\pi\} \tag{1}$$

where $\#\{\cdot\}$ stands for "cardinality of" and S_π is the set formed by the elements of S that are invariant under permutation π. For the purpose of particularizing the general statement of the theorem to the case of circular binary patterns, it is insightful to translate the mathematical jargon to common language as well as to identify the different terms in Eq. 1. Thus, the cardinality of the quotient set S/G is simply the number of different rotation invariant circular binary patterns, i.e., the number of histogram bins of the texture model considered. The permutation group G is the set of all the rotations that a circular pattern can undergo, namely π_0, π_{45}, π_{90}, π_{135}, π_{180}, π_{225}, π_{270} and π_{315}, corresponding to rotation angles of 0º, 45º, 90º, 135º, 180º, 225º, 270º and 315º, respectively. Hence, $\#\{G\} = 8$. To alleviate notation we write p_α to denote $\#\{S_{\pi_\alpha}\}$, i.e., the number of circular binary patterns that remain unchanged after a rotation by α degrees. The dimensionalities of the LBP, CCR and ILBP rotation invariant feature spaces can be obtained through the following formula:

$$\frac{(p_0 + p_{45} + p_{90} + p_{135} + p_{180} + p_{225} + p_{225} + p_{270})}{8} \tag{2}$$

Let us first consider the LBP model. Trivially, $p_0 = 2^8$, since there are 256 different LBP patterns, and all of them remain the same after a 0 degrees rotation. Also trivially, $p_{45} = p_{135} = p_{225} = p_{315} = 2$, since the only invariant patterns against rotation by 45º, 135º, 225º and 315º are the constant patterns. Let us now unwrap the circular binary patterns to form binary strings. A counter-clockwise rotation of the circular pattern by an angle of $45 \times n$ degrees is equivalent to a circular shift of n positions leftwards to the string, where n being a natural number. Taking this into account, one can readily ascertain that 01010101, 10101010 and the constant patterns are the only patterns that remain unchanged after rotation by either 90º or 270º, and hence, $p_{90} = p_{270} = 4$. Let $b_7 b_6 b_5 b_4 b_3 b_2 b_1 b_0$ be a generic 8-bit binary pattern, with $b_j \in \{0, 1\}\ \forall j$, and let $b_3 b_2 b_1 b_0 b_7 b_6 b_5 b_4$ the same pattern after a 180º rotation. The original pattern is invariant against 180º rotation if and only if the following conditions are simultaneously fulfilled: $b_7 = b_3$, $b_6 = b_2$, $b_5 = b_1$ and $b_4 = b_0$. There are obviously 2^4 solutions for this binary-valued system of four parametric equations, and therefore $p_{180} = 16$. Introducing all these values in Eq. 2 yields:

$$\#\{\mathrm{LBP}^{ri}_{8,1}\} = \frac{(256 + 2 + 4 + 2 + 16 + 2 + 4 + 2)}{8} = 36 \tag{3}$$

Considering that if we enhance an 8-bit LBP circular patterns by adding the central pixel we get two 9-bit CCR circular patterns, and following a reasoning analogous to the one exposed in the preceding paragraph, one can derive the number of rotation invariant circular patterns corresponding to the CCR texture model:

$$\#\{\mathrm{CCR}^{ri}_{8,1}\} = \frac{(512 + 4 + 8 + 4 + 32 + 4 + 8 + 4)}{8} = 72 \tag{4}$$

Finally, it is convenient to recall that the constant pattern formed by all 0's is —by definition— impossible in the ILBP model, and as a result the dimensionality of the $\mathrm{ILBP}^{ri}_{8,1}$ feature space is:

$$\#\{\mathrm{ILBP}^{ri}_{8,1}\} = \frac{(511 + 3 + 7 + 3 + 31 + 3 + 7 + 3)}{8} = 71 \tag{5}$$

A side effect of the above described rotation-invariant operators is an increase of the frequency of constant patterns. If we consider, for instance, the texture *Azul Platino*, the occurrence of such patterns represents 58.9% and 8.4% of the $\mathrm{CCR}_{3\times3}$ and $\mathrm{LBP}_{3\times3}$ histograms, respectively (Figs. 1(d) and 1(a)). In the case of the $\mathrm{CCR}^{ri}_{8,1}$ and $\mathrm{LBP}^{ri}_{8,1}$ these proportions rise to 67.0% and 10.4%, respectively (Figs. 1(e) and 1(b)). We believe that such a discrepancy between the basic and the rotation invariant versions is due to the conversion of squared neighbourhoods into circular neighbourhoods through bilinear interpolation, that might convert a number of non-constant square patterns into constant circular patterns.

The dimension of the feature space can be further reduced by introducing the concept of uniformity. A local binary pattern is considered *uniform* when the number of transitions in the circular bitwise presentation of the LBP code is at most two [30]. The term refers to the uniform appearance of such patterns, which arises from the limited number of black-white or white-black transitions. Researchers at the University of Oulu, Finland, found that the uniform patterns represent the vast majority of the 3×3 local binary patterns in surface textures [33]. Although the use of uniform patterns provides the beneficial advantage of a low-dimensional feature space, recent results suggest that this approach has some significant shortcomings, since it discards some important

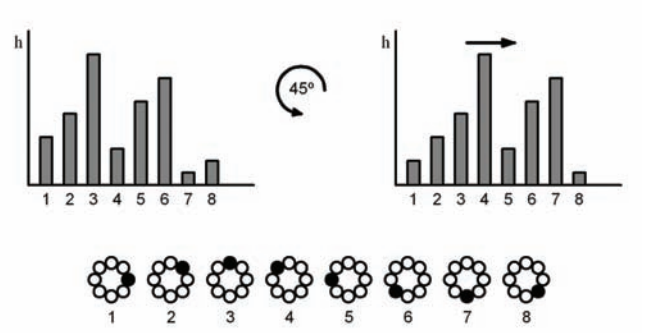

Fig. 3 Texture rotation introduces a circular shift in each subset of bins which represent rotationally-equivalent patterns.

texture information and it is sensitive to noise [53]. It has also been reported that in those textures whose edges and shapes are not regular (like granite texture) the dominant patterns are not mainly the uniform ones [28,29], and therefore it is recommendable, in such cases, to use all the LBP patterns. Based on these considerations we decided not to use uniform patterns in our experimental activity.

3.2 Discrete Fourier Transform

The Discrete Fourier Transform is a common method to obtain rotation invariant texture features. It can be virtually applied to any feature space that holds the circular shift property, that is: a rotation of the texture results in a circular shift of the feature vector. This method has been successfully used within many texture descriptors, such as Gabor filters [21,6], Markov Random Fields [10], ridgelet features [9], and Radon transform [52]. A DFT-based approach for rotation invariant LBP features has been recently presented in [1]. Unfortunately this method computes rotation invariant features from the histogram of uniform LBP patterns, which are not adequate to the application studied in this paper, due to the considerations presented in the previous section. Therefore we adopted a generalization of the method presented in [1], with the difference that rotation invariant features are obtained through DFT normalization of the original $\mathrm{LBP}_{8,1}$ histogram. We also extend this method to the other feature spaces considered, namely ILBP and CCR. The approach is described below.

Let's begin with the case of LBP. Let's consider a circular binary pattern, its rotated versions, and the probability of occurrence of the pattern itself and its rotated versions. We can observe that, as the texture rotates by 45°, the corresponding histogram bins undergo a circular shift by one position (Fig. 3). In formulas: if $\mathbf{x}_\theta = \{x_1, \cdots, x_N\}$ is the set of values of the probability of occurrence of a pattern and its rotated versions at a given texture angle θ, after a texture rotation by 45° this set of bins becomes $\mathbf{x}_{\theta+45^\circ} = \{x_N, x_1, \cdots, x_{N-1}\}$. As a consequence a rotation invariant version of the vector $\mathbf{x}$ can be obtained by taking the discrete Fourier transform. If $\mathbf{X} = [X_0, X_1, \ldots, X_{N-1}]$ is the DFT of $\mathbf{x}$, the moduli of the transformed coefficients $|X_k|$ are independent of any circular shift of the input vector $\mathbf{x}$. In addition, knowing that the DFT output is half redundant, we get the complete information by looking at the first $[(N/2)+1]$ elements of the transformed vector [6], where $[\cdot]$ denotes "integer part of". In summary, the algorithm to obtain the rotational invariant LBP involves the following operations:

1. Compute the original $\mathrm{LBP}_{8,1}$ histogram:
$$\mathbf{h} = \{h_1, \cdots, h_{256}\} \tag{6}$$
2. Remove the first and the last bins of the histogram (they represent the all-black and all-white constant patterns):
$$\mathbf{h}' = \{h_2, \cdots, h_{255}\} \tag{7}$$
3. Rearrange the resulting LBP histogram in blocks of bins so that each block refers to rotationally-equivalent patterns:
$$\mathbf{h}' = \{\mathbf{h}_1, \cdots, \mathbf{h}_M\} \tag{8}$$
where, $\mathbf{h}_i = \{h_{i1}, \cdots, h_{iN}\}$ and $M = 34$. It should be observed that this value results of borrowing 2 from Eq. 3. We can imagine each group of rotation invariant patterns as formed by a *basic pattern* and all its rotated versions. In addition, for the circular shift property to be satisfied, we order each group of bins which refers to a group of rotation invariant patterns in such a way that if the h_{i1} bin refers to the basic pattern, the h_{i2} bin refers to the pattern obtained through a single rotation of 45° from the basic pattern, and so on. In general each group is composed of eight different rotationally-equivalent patterns (therefore $N = 8$). But, as discussed in Section 3.1, in some cases the number of different patterns for group is less than eight. This occurs when a rotated version of a pattern coincides with the unrotated version: if the basic pattern has the form 00010001, 00110011 or 01110111 then $N = 4$; if it has the form 01010101 then $N = 2$.
4. Compute the DFT $\mathbf{H}_i$ of each $\mathbf{h}_i$ and retain only the moduli of the first $[(N/2)+1]$ elements of each $\mathbf{H}_i$.
5. Normalize the elements of each $\mathbf{H}_i$ so that the energy of the transformed coefficients equals the energy of the original bin values:
$$\overline{\mathbf{H}}_i = c_i \mathbf{H}_i \tag{9}$$
where
$$c_i = \frac{\sum_{k=1}^{N} h_{ik}}{\sum_{k=1}^{[(N/2)+1]} H_{ik}} \tag{10}$$

6. Obtain the rotation invariant feature vector: $\mathbf{H} = \{\overline{\mathbf{H}}_1, \cdots, \overline{\mathbf{H}}_M\}$;
7. Add to the above feature vector the first and last elements of the histogram that were previously removed in step (2).

The resulting feature space is denoted by $\mathrm{LBP}^{DFT}_{8,1}$. The method can be immediately extended to the CCR and ILBP models if we consider that a CCR histogram can be split into two LBP histograms: one that accounts for all the texels whose central pixel value is 0, and the other that accounts for all the texels whose central pixel value is 1. The corresponding feature spaces are denoted by $\mathrm{ILBP}^{DFT}_{8,1}$ and $\mathrm{CCR}^{DFT}_{8,1}$, respectively.

It is worth mentioning that the DFT-based method can be considered as a generalization of the method based on rotation invariant patterns, which has been presented in section 3.1. This is motivated by the following observation: by only retaining the DC component of the DFT-transformed bins we obtain the texture-based approach based on rotationally invariant patterns.

4 Overview of the image acquisition set-up

The visual appearance of a particular granite strongly depends on the surface roughness. Common finishes include sawn, flamed, bush-hammered, honed and polished, which is the most extended one and dominates the market. The usual procedure to obtain a polished finish involves two operations: first, the granite slab is subject to the action of a rotating disc impregnated with abrasive powder, and second, the remaining pores and scratches are sealed with polish wax. As a result of it, the full colour and crystal structure of the stone become visible, and the surface acquires a glossy appearance. This mirror like finish is a major issue for a machine vision system. To tackle the problem of specular reflections, special care has to be taken in recording images. The stone surface has to be optically shielded in order to avoid, on the one hand, the influence of environmental light fluctuations, and on the other hand, overlapping between the granite texture and the reflected image of the scene in front of the granite slab. In addition, completely diffuse illumination is required to ensure that light intensity is uniformly distributed all over the field of view, and thus the image is free of shadows and specular reflections.

The imaging system used to capture the granite image data consists of a LED ring light mounted on the base of an opaque, hemispherical dome of 46.5 cm diameter (see Fig. 4(a)) whose inner wall is coated with a material that approximates to the ideal Lambertian scatterer. The light rays incident on any point of the stone surface are, by multiple scattering reflections, distributed equally to all other such points, and therefore provide even illumination on the granite slab. The dome has a through hole on top which allows observation of the specimen. Colour texture images were recorded using a consumer digital still camera (*Samsung S850*), which is rigidly attached to the dome in order to keep constant the distance from the camera to the stone surface, and therefore the image scale, during the image acquisition process. The dome is mounted on a special support (see Fig. 4(b)) that makes it possible to change the relative rotation between the camera and the granite tile to be acquired. The mounting device supports the same set of rotation angles used in [35]: 0°, 5°, 10°, 15°, 30°, 45°, 60°, 75° and 90°.

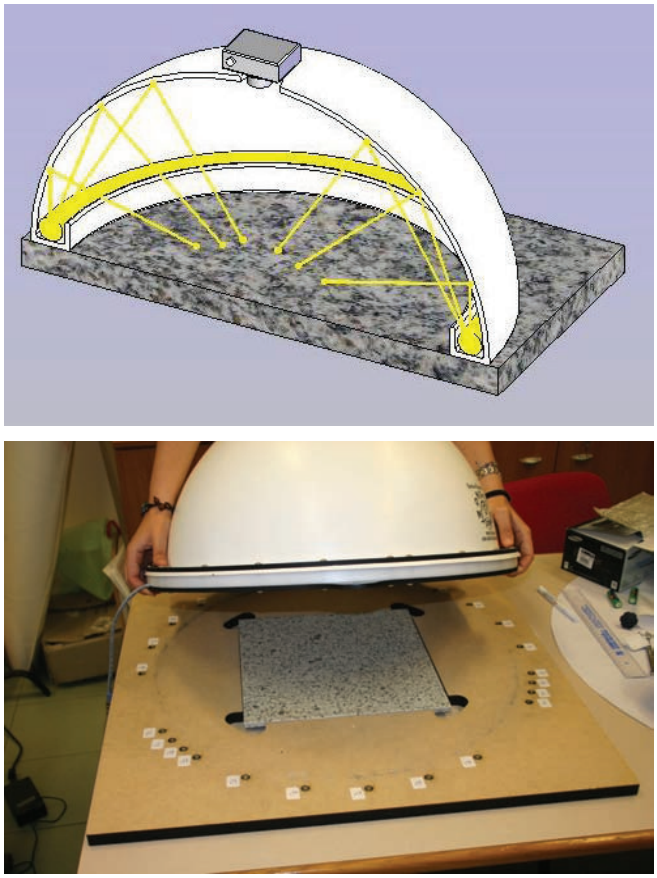

Fig. 4 (a) Illumination system inside the dome. **(b)** The dome together with the support that makes it possible to take images of the granite tiles at different rotation angles

Moreover, in order to ensure that all the images were recorded under the same conditions, we disabled the automatic gain control of the camera, and manually set the resolution, the shutter speed, the f-stop and the ISO to the following values: 1024×768, 1/30 s, 7.4 and 50, respectively.

Fig. 5 The dataset of granite textures used in the experiments (unrotated images). From the top: *Acquamarina*, *Azul Capixaba*, *Bianco Cristal*, *Bianco Sardo*, *Rosa Beta*, *Azul Platino*, *Giallo Ornamentale*, *Giallo Napoletano*, *Giallo Santa Cecilia*, *Giallo Veneziano*, *Rosa Porriño A*, *Rosa Porriño B*.

5 Assessment of robustness

5.1 Benchmark data

Experimental evaluation of texture classification accuracy has been performed over a set of 12 types of commercial varieties of granite (Fig. 5), namely: *Acquamarina*, *Azul Capixaba*, *Azul Platino*, *Bianco Cristal*, *Bianco Sardo*, *Giallo Napoletano*, *Giallo Ornamentale*, *Giallo Santa Cecilia*, *Giallo Veneziano*, *Rosa Beta*, *Rosa Porriño A*, *Rosa Porriño B*. The granite tiles comes from a stone manufacturing company *Mondial Marmi SpA* (Perugia, Italy). The overall dataset is composed of 48 images, 4 for each class. It should be noted that such granite classes represent a challenging dataset, since many of them exhibit similar visual characteristics.

The texture images were acquired under controlled conditions using the system described in the preceding section. To assess robustness against rotation we used both hardware- and software-rotated images. Hardware-rotated images have been acquired using all the rotation angles provided by the mounting system, namely: 0°, 5°, 10°, 15°, 30°, 45°, 60°, 75° and 90°. This results in a database of 432 images (48 for each rotation angle). Software-rotated images have been obtained by rotating the 0° image by the same angles. Two approaches have been used to image rotation by software: *bilinear* and *bicubic* interpolation. In both cases we used the function `imrotate` of the Matlab package. Finally, in consideration of the fact that, as the granite surface rotates, only the central part of the image captures the same portion of the surface, we only retained the central part of the original images. If W and H are the width and height of the original image, the area to be retained is a centered square the dimension of which is $min(W, H)/\sqrt{2}$. This gives an image size of 544 x 544 pixels.

5.2 Procedure

The index considered here to assess feature robustness against rotation is the percentage of correctly classified textures in a supervised learning task. The classification experiments were based on the nearest neighbour rule [11] with the L_1 norm, also called Manhattan distance. Classification error has been evaluated by *split-half validation* with *stratified sampling* [8]. This means that the dataset was randomly subdivided into two subsets, one used for training (*training set*), and the other for testing (*validation set*). Moreover, the proportion of examples of each class in the training set is maintained the same to avoid class biasing in the classification process. In order to assess robustness against rotation, the training set is always composed of textures picked from the 0° group, while the validation set is composed of rotated versions of textures taken from the θ degrees group, with $\theta \in \{0°, 5°, 10°, 15°, 30°, 45°, 60°, 75°, 90°\}$. For each rotation

angle we averaged the results obtained over 100 different random partitions into training and validation set to have a stable estimation of the generalization error. To make things clearer, the per-unit version of the index we use to assess the classification accuracy obtained for a texture rotation of θ degrees can be formalized as follows:

$$A_\theta = \frac{\sum_{j=1}^{100} \frac{A_{\theta,j}}{24}}{100} \tag{11}$$

where $A_{\theta,j}$ denotes the number of correct classifications achieved for a rotation angle θ by using the jth random partition of the 48 images that compose the dataset, that is to say, when the classifier is trained with 24 unrotated images (2 samples per granite class) and the validation is perfomed over the remaining 24 images (also 2 samples per granite class) after being rotated by θ degrees.

5.3 Experimental results and discussion

The results of the experimental activity are summarized in Table 1. The table is organized as follows: the first column reports the feature space, the second column the dimension of the feature space, the third column the method used to rotate textures; the columns from A_{0^o} to A_{90^o} the percentage of correct classification obtained when the rotation angle of the textures of the validation set varies from 0° to 90°. Finally the column *mean* reports the mean classification accuracy over the nine rotation angles considered, and the column *st_dev* the standard deviation of the accuracy over the nine rotation angles.

In order to draw meaningful conclusions from the experimental activity, it is convenient to separately analyse the results obtained with hardware-rotated images and those obtained with software-rotated images. In the first case we can conclude the following: the original (non rotation-invariant) versions of the methods (namely: $\text{LBP}_{3\times3}$, $\text{ILBP}_{3\times3}$, and $\text{CCR}_{3\times3}$) are not invariant against rotation, as one would expect. On the contrary all the rotation-invariant versions of the analysed features proved to be robust against rotation and they should theoretically return similar performance irrespective of the orientation angle. However, it is useful to note that the CCD or CMOS sensors are defined by an ordered structure of either rectangular or square pixels. Since the pixels that form the sensing element do not have circularly symmetric shapes, small aliasing effects are inserted during the image acquisition process if the image is rotated with angles that are not orthogonal to the original position (0 degrees). Based on this observation, it is expected that the classification errors peak when the images are rotated by 45 degrees since the aliasing effects are maximised for this orientation.

A different scenario emerges if we use software-rotated textures. In this case the experimental results show that not only the original versions of the methods are not robust against rotation, but also their rotation invariant versions are not. At a first glance these results could appear somewhat surprising. However we have to consider that rotation by software attenuates high frequency components of the image [23], and therefore some information is lost in the process. Such smoothing considerably alters the intrinsic texture structure, since it wipes out the micro-textural data. This observation is supported by the experimental results depicted in Table 1, where it can be observed that the classification results achieved by the rotationally invariant descriptors (ri and DFT) for 90 degrees synthetically rotated data closely match the classification results obtained at 0 degrees. These results are motivated by the fact that no interpolation is required for orthogonal rotations (90, 180 and 270 degrees), since the image rotation for these orientations involves one-to-one pixel mapping. Fig. 7 gives an example of the changes which may suffer a gray-scale pattern when rotated by 5° through bilinear interpolation. As we can see, even a small rotation angle can induce changes in the corresponding local binary pattern, which are likely to degrade the classification accuracy.

The last point worth commenting on is that experimental results show that $\text{CCR}_{3\times3}$ model is more robust against rotation than $\text{LBP}_{3\times3}$, while the opposite holds true for the rotation invariant versions of these descriptors. We believe that the intrinsic robustness of the basic $\text{CCR}_{3\times3}$ is motivated by the conspicuous peaks located at both extremes of the histogram (see Fig. 1(d)), which indicate that the vast majority of the binary patterns are constituted by all 0's and all 1's, i.e., are constant patterns. This means that classification is strongly dominated by the occurrence frequency of the constant patterns, which is fairly independent of rotation. The use of rotation invariant versions, namely $\text{CCR}_{8,1}^{ri}$ and $\text{CCR}_{8,1}^{DFT}$, attenuates the relative weight of the constant patterns on the overall histogram, and as a result of it, the average performances of both LBP and CCR models become comparable.

6 Conclusions

In this work we evaluated the robustness against rotation of the LBP, ILBP and CCR texture models in the context of granite texture classification. Granite texture is traditionally considered hard to classify, due to its highly stochastic and irregular nature. To this end, we carried out a large number of experiments using a dataset of hardware- and software-rotated granite textures acquired under controlled conditions. We assessed the robustness against rotation of LBP, ILBP and CCR features, in their basic forms as well as their rotation invariant versions. Rotation invariance has been obtained in

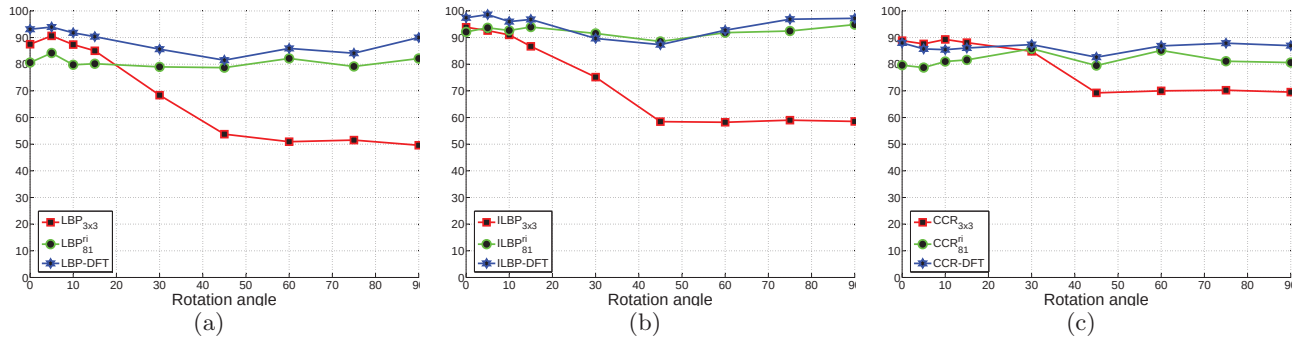

Fig. 6 Plots of A_θ (expressed in %) corresponding to hardware-rotated textures: **(a)** LBP, **(b)** ILBP and **(c)** CCR.

Table 1 Results of the experimental activity. Accuracies are expressed as percentages.

Feature space	Dim	Rotation	Mean	*St_dev*	$A_{0°}$	$A_{5°}$	$A_{10°}$	$A_{15°}$	$A_{30°}$	$A_{45°}$	$A_{60°}$	$A_{75°}$	$A_{90°}$
$\mathbf{LBP}_{3\times3}$	256	hardware	**69,4**	*18,2*	87,5	90,6	87,4	85,0	68,4	53,8	50,9	51,5	49,6
		bilinear	**36,5**	*20,5*	87,5	31,7	30,2	27,9	26,5	25,4	25,6	25,0	49,0
		bicubic	**44,7**	*17,9*	87,5	46,5	47,2	44,0	38,6	30,8	30,9	28,1	49,0
$\mathbf{LBP}^{ri}_{8,1}$	36	hardware	**80,7**	*1,8*	80,6	84,2	79,8	80,2	79,0	78,7	82,2	79,2	82,1
		bilinear	**37,4**	*24,5*	80,6	25,0	25,0	25,0	25,0	25,0	25,0	25,0	80,6
		bicubic	**41,5**	*22,2*	80,6	29,0	28,9	28,9	31,7	31,9	33,0	28,9	80,6
$\mathbf{LBP}^{DFT}_{8,1}$	163	hardware	**88,5**	*4,3*	93,1	94,0	91,8	90,3	85,6	81,5	85,9	84,1	90,0
		bilinear	**41,6**	*29,2*	93,1	27,0	28,7	27,6	25,5	25,8	26,1	27,1	93,1
		bicubic	**56,8**	*20,7*	93,1	45,0	45,3	45,5	45,2	46,5	48,5	48,7	93,1
$\mathbf{ILBP}_{3\times3}$	511	hardware	**74,8**	*16,4*	93,9	92,6	91,0	86,7	75,2	58,5	58,2	59,0	58,5
		bilinear	**48,7**	*18,9*	93,9	48,5	48,9	45,0	38,4	39,4	34,8	30,7	58,4
		bicubic	**60,3**	*15,8*	93,9	69,2	67,4	63,1	55,7	47,5	45,3	42,5	58,4
$\mathbf{ILBP}^{ri}_{8,1}$	71	hardware	**92,4**	*1,8*	92,1	93,7	92,7	94,0	91,5	88,5	91,8	92,5	94,9
		bilinear	**51,3**	*23,2*	92,1	38,7	39,2	40,0	39,3	41,7	39,8	38,8	92,1
		bicubic	**59,0**	*18,8*	92,1	47,1	47,9	48,5	51,7	51,2	51,3	49,3	92,1
$\mathbf{ILBP}^{DFT}_{8,1}$	325	hardware	**94,7**	*3,9*	97,4	98,6	96,0	96,8	89,7	87,3	92,8	96,9	97,2
		bilinear	**58,9**	*22,0*	97,4	49,0	50,5	50,7	44,0	42,5	47,9	51,0	97,4
		bicubic	**72,1**	*15,5*	97,4	70,7	70,3	69,1	59,3	54,1	61,0	69,5	97,4
$\mathbf{CCR}_{3\times3}$	512	hardware	**79,7**	*9,6*	88,8	87,6	89,3	88,1	84,8	69,3	70,0	70,3	69,5
		bilinear	**48,2**	*17,6*	88,8	43,0	44,2	43,6	43,0	40,0	34,7	32,5	63,7
		bicubic	**68,5**	*12,6*	88,8	75,2	77,8	77,1	71,7	55,6	53,9	53,1	63,7
$\mathbf{CCR}^{ri}_{8,1}$	72	hardware	**81,5**	*2,5*	79,6	78,8	81,0	81,6	85,8	79,5	85,2	81,1	80,6
		bilinear	**50,4**	*16,6*	79,6	41,4	43,6	43,9	43,4	41,1	40,8	39,9	79,6
		bicubic	**66,6**	*7,6*	79,6	61,3	60,0	64,1	64,6	62,5	66,4	61,4	79,6
$\mathbf{CCR}^{DFT}_{8,1}$	326	hardware	**86,3**	*1,7*	88,0	85,7	85,5	86,1	87,4	82,6	86,9	87,9	87,0
		bilinear	**53,2**	*19,7*	88,0	42,3	44,0	44,3	44,2	42,4	42,5	43,2	88,0
		bicubic	**75,3**	*7,3*	88,0	72,0	73,2	72,3	71,7	69,3	73,0	70,6	88,0

two different ways: through rotation invariant patterns, as proposed in [31], and through the Discrete Fourier Transform. We provided a description of this new method in section 3.2.

Among the three texture models, the ILBP provided significantly higher results, whereas the performances obtained with the LBP and the CCR are comparable. The analysis of robustness against rotation generated different outcomes, depending on the method used to rotate the images. With hardware-rotated images the rotation invariant methods show good robustness against rotation. A comparison of the two approaches shows that the DFT performs better. This result is logical, since this method can be considered an extension of the approach based on rotationally invariant patterns. On the contrary the robustness against rotation is poor when considering software-rotated images. We gave an explanation of this result in the previous section. This suggests that experimental results obtained using software-rotated images should be carefully considered, since they may lead to misleading conclusions.

Acknowledgements The authors would like to acknowledge the anonymous reviewers for their constructive comments. This research was funded by Xunta de Galicia under the grant n. PGIDIT04REM303003PR and by the Fondazione CARIT (Terni, Italy) under the project entitled "*Sviluppo di metodologie di simulazione del comportamento di materiali impiegati nell'edilizia e nell'industria meccanica*". The authors are grateful to INFAIMON, S.L. for providing the dome

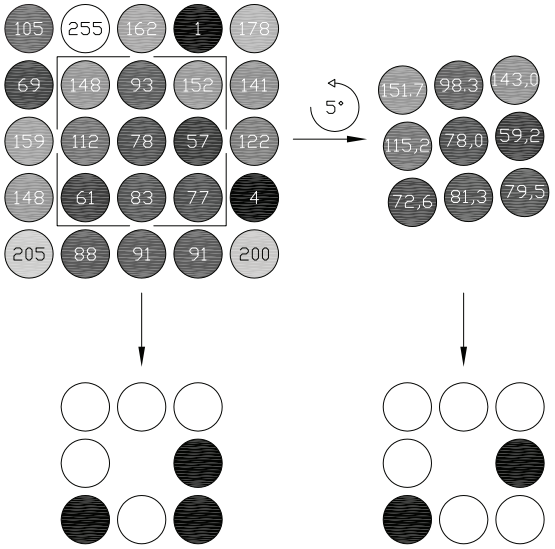

Fig. 7 An example of the effects of software rotation through bilinear interpolation on the texture structure. Even a small rotation angle may induce changes in the LBP code of a gray-scale pattern.

used to illuminate the granite slabs and to Mondial Marmi SpA for providing the granite tiles used in the experiments. Antonio Fernández thanks the University of Vigo for support during his sabbatical year, at which time part of this work was performed. Francesco Bianconi thanks the University of Vigo for a travel fellowship. And last, but not least, Antonio Fernández is grateful to Pablo and Ana for their hospitality during his stay in Dublin.

References

1. Ahonen, T., Matas, J., He, C., Pietikäinen, M.: Rotation Invariant Image Description with Local Binary Pattern Histogram Fourier Features. Lect Notes Comput Sc **5575**, 61–70 (2009)
2. Baxter, M.: The Burnside Di-Lemma: Combinatorics and Puzzle Symmetry. In: Cipra, B., Demaine, E.D., Demaine, M.L., Rodgers, T. (eds.), Tribute to a mathemagician, A K Peters Ltd, Wellesley, MA, pp. 199–210 (2005)
3. Bennamoun, M., Bodnarova, A.: Digital image processing techniques for automatic textile quality control. Syst Anal Model Sim **43**, 1581–1614 (2003)
4. Bianconi, F., Fernández, A.: Granite texture classification with Gabor filters. In: Proc. of the 18th International Congress on Graphical Engineering, Sitges (Spain), May 31 - June 2, (2006)
5. Bianconi, F., Fernández, A., González, E., Ribas F.: Texture classification through combination of sequential colour texture classifiers. Lect Notes Comput Sc **4756**, 231–240 (2007)
6. Bianconi, F., Fernández, A., Mancini, A.: Assessment of rotation-invariant texture classification through Gabor filters and Discrete Fourier Transform. In: Proc. of the 20th International Congress on Graphical Engineering, Valencia (Spain), June 4-6, (2008)
7. Bianconi, F., Fernández, A., González, E., Caride, J., Calviño, A.: Rotation-invariant colour texture classification through multilayer CCR. Pattern Recogn Lett **30**, 765–773 (2009)
8. Braga-Neto, U., Dougherty, E.: Exact performance of error estimators for discrete classifiers. Pattern Recogn **38**, 1799–1814 (2005)
9. Chen, G.Y., Bui, T.D., Kryzak, A.: Invariant Ridgelet-Fourier Descriptor for Pattern Recognition. In: Proc. of the 18th International Conference on Pattern Recognition, Hong Kong, August 20-24, 768–771 (2006)
10. Deng, H., Clausi, D.A.: Gaussian MRF rotation-invariant features for image classification. IEEE T Pattern Anal **26**, 951–955 (2004)
11. Duda, R.O., Hart, P.E., Stork, D.G.: Pattern Classification. Wiley-Interscience, New York (2001)
12. Standard EN 12440:2000: Natural Stone - Denomination Criteria
13. Ghita, O., Whelan, P.F., Carew, T., Nammalwar, P.: Quality grading of painted slates using texture analysis. Comput Ind **56**, 802–815 (2005)
14. Guillén-Bonilla, J.T., Kurmyshev, E.V., Fernández, A.: Quantifying a similarity of classes of texture images. Appl Opt **46**, 5562–5570 (2007)
15. Hoang, K., Wen, W., Nachimuthu, A., Jiang, X.L.: Achieving automation in leather surface inspection. Comput Ind **34**, 43–54 (1997)
16. Jin, H., Liu, Q., Tong, X.: Face Detection Using Improved LBP Under Bayesian Framework. In: Proc. of the 3rd International Conference on Image and Graphics, 306–309 (2004)
17. Kirsanova, E.N., Sadovsky, M.G.: Entropy Approach in the Analysis of Anisotropy of Digital Images. Open Systems and Information Dynamics, **84**, 239–250 (2002)
18. Kukkonen, S., Kälviäinen, H., Parkkinen, J.: Color features for quality control in ceramic tile industry. Opt Eng **40**, 170–177 (2001)
19. Kurmyshev, E.V., Cervantes, M.: A quasi-statistical approach to digital image representation. Rev Mex Fis **42**, 104–116 (1996)
20. Kurmyshev, E., Poterasu, M., Guillén-Bonilla, J.T.: Image Scale determination for Optimal Texture Classification using Coordinated Cluster Representation. Appl Optics **46**, 1467–1476 (2007)
21. Lahajnar, F., Kovacic, S.: Rotation-invariant texture classification, Pattern Recogn Lett **5575**, 1151–1161 (2003)
22. Larabi, M., Colot, O., Richard, N., Fernandez-Maloigne, C.: Using a CBIR Scheme Based on Experts Knowledge for a Computer-Aided Classification of Ornamental Stones. In: Proc. of the 6th International Conference on Quality Control by Artificial Vision, Gatlinburg (USA), May 19-23, 189–200 (2003)
23. Larkin, K.G., Oldfield, M.A., Klemm, H.: Fast Fourier method for the accurate rotation of rotation of sampled images. Optics Communications **139**, 99–106 (1997)
24. Lepistö, L., Kunttu, I., Visa, A.: Rock image classification using color features in Gabor space. J Electron Imaging **14**, 040503-1-3 (2005)
25. Lepistö, L., Kunttu, I., Visa, A.: Color-Based Classification of Natural Rock Images Using Classifier Combinations. Lect Notes Comput Sc **3540**, 901–909 (2005)
26. Lepistö, L., Kunttu, I., Visa, A.: Rock image classification based on k-nearest neighbour voting. IEE P-Vis Image Sig **153**, 475–482 (2006)
27. Lepistö, L., Kunttu, I., Visa, A.: Classification of natural rock images using classifier combinations. Opt Eng **45-9**, 097201-1-7 (2006)
28. Liao, S., Law, W.K., Chung, A.C.S.: Combining Microscopic and Macroscopic Information for Rotation and Histogram Equalization Invariant Texture Classification. Lect Notes Comput Sc **3851**, 100–109 (2006)

29. Liao, S., Chung, A. C. S.: Texture Classification by using Advanced Local Binary Patterns and Spatial Distribution of Dominant Patterns. In: Proc. IEEE International Conference on Acoustics, Speech and Signal Processing (ICASSP 2007), vol. I, pp. 1221–1224 (2007)
30. Mäenpää, T., Ojala, T., Pietikäinen, M., Soriano, M.: Robust texture classification by subsets of Local Binary Patterns. In: Proc. 15th International Conference on Pattern Recognition, Barcelona (Spain), vol. 3, pp. 947–950 (2000)
31. Mäenpää, T., Pietikäinen, M.: Texture analysis with local binary patterns. In: Chen, C. H., Wang, P. S. P. (eds.), The Handbook of Pattern Recognition and Computer Vision, World Scientific Publishing, Singapore, pp. 197–216 (2005)
32. Martínez-Alajarín, J., Luis-Delgado, J.D., Tomás-Balibrea, L.M.: Automatic System for Quality-Based Classification of Marble Textures. IEEE T Syst Man Cy C **35**, 488–497 (2005)
33. Ojala, T., Pietikäinen, M., Harwood, D.: A comparative study of texture measures with classification based on feature distributions. Pattern Recogn **29**, 51–59 (1996)
34. Ojala, T., Pietikäinen, M., Mäenpää, T.: Multiresolution Gray-Scale and Rotation Invariant Texture Classification with Local Binary Patterns. IEEE T Pattern Anal **24**, 971–987 (2002)
35. Ojala, T., Mäenpää, T., Pietikäinen, M., J. Viertola, Kyllönen, J., Huovinen, S.: Outex—new framework for empirical evaluation of texture analysis algorithms. In: Proc. of the 16th International Conference on Pattern Recognition, Quebec (Canada), pp. 701–706 (2002)
36. Paclík, P., Verzakov, S., Duin, R.P.W.: Improving the maximum-likelihood co-occurrence classifier: A study on classification of inhomogeneous rock images. Lect Notes Comput Sc **3540**, 998–1008 (2005)
37. Partio, M., Cramariuc, B., Gabbouj, M., Visa, A.: Rock texture retrieval using gray level co-occurence matrix. In: Proc. of the 5th Nordic Signal Processing Symposium, 2002 (NORSIG 2002), on board Hurtigruten (Norway), 4-7 October (2008)
38. Paschos, G.: Fast color texture recognition using chromaticity moments. Pattern Recogn Lett **21**, 837–841 (2000)
39. Porter, R., Canagarajah, N.: Robust rotation-invariant texture classification: wavelet, Gabor filter and GMRF based schemes. IEE P-Vis Image Sig **144**, 180–188 (1997)
40. Rubner, Y., Puzicha, J., Tomasi, C., Buhmann, J.M.: Empirical Evaluation of Dissimilarity Measures for Color and Texture. Comput Vis Image Und **84**, 25–43 (2001)
41. Sánchez-Yáñez, R.E., Kurmyshev, E.V., Cuevas, F.J.: A framework for texture classification using the coordinated clusters representation. Pattern Recogn Lett **24**, 21–31 (2003)
42. Sánchez-Yáñez, R.E., Kurmyshev, E.V., Fernández, A.: One-class texture classifier in the CCR feature space. Pattern Recogn Lett **24**, 1503–1511 (2003)
43. Sezgin, M., Sankur, B.: Survey over image thresholding techniques and quantitative performance evaluation. J Electron Imaging **13**, 146–165 (2004)
44. Shadmon, A.: Stone Absolute (by any other name). Litos **78** (2005)
45. Silvén, O., Niskanen, M., Kauppinen, H.: Wood inspection with non-supervised clustering. Mach Vision Appl **13**, 275–285 (2003)
46. Tan, T.S.C., Kittler, J.: Colour texture analysis using colour histogram. IEE P-Vis Image Sig **141**, 403–412 (1994)
47. Turtinen, M., Pietikäinen, M., Silvén, O., Mäenpää, T., Niskanen, M.: Paper characterisation by texture using visualisation-based training. Int J Adv Manuf Tech **22**, 890–898 (2003)
48. Wang, L., He, D.C.: Texture classification using texture spectrum. Pattern Recogn **23**, 905–910 (1990)
49. Weisstein, E.W.: CRC Concise Encyclopedia of Mathematics, Second Edition. CRC Press (2002)
50. Xie, X., Mirmehdi, M.: A Galaxy of Texture Features. In: Mirmehdi, M., Xie, X., Suri, J. (eds.), Handbook of Texture Analysis, Imperial College Press, London, pp. 347–406 (2008)
51. Yao, C.H., Chen, S.Y.: Retrieval of translated, rotated and scaled color textures. Pattern Recogn **36**, 913–929 (2003)
52. Yu, G., Cao, W., Li, Z.: Rotation and Scale Invariant for Texture Analysis Based on Radon Transform and Wavelet Transform. In: Proc. of the 3rd International Conference on Pervasive Computing and Applications, Alexandria (Egypt), 6-8 October, 704–708 (2008)
53. Zhou, H., Wang, R., Wang, C.: A novel extended local-binary-pattern operator for texture analysis. Information Sciences, **178**, 4314–4325 (2008)

Antonio Fernández graduated as an industrial engineer in 1993 and obtained the Ph.D. degree in industrial engineering (with special distinction) in 1998, both from the University of Vigo, Spain. He is currently a senior lecturer in the Department of Engineering Design, and the Head of the Colorimetry Research Group. He has worked as a visiting researcher at Centre for Research on Optics (Mexico), University of Perugia (Italy), Dublin City University (Ireland) and Computer Vision Centre (Spain). His major research interests include texture analysis and speckle metrology.

Ovidiu Ghita received his B.E. and M.E. degrees in Electrical Engineering from Transilvania University, Brasov, Romania. From 1994 through 1996 he was an Assistant Lecturer in the Department of Electrical Engineering at Transilvania University. Since then, he has been a member of the Vision Systems Group at Dublin City University (DCU), during which time he received his Ph.D. for work in the area of robotic vision. Currently, he holds a position of Postdoctoral Research Fellow in the Vision Systems Group at DCU. Dr. Ghita has authored and co-authored more than 60 peer-reviewed research papers in areas of machine vision, range acquisition, instrumentation and medical imaging.

Elena González received her B.Sc. and Ph.D. in industrial engineering in 1985 and 1994, respectively, from the University of Vigo, Spain, where she is currently a senior lecturer with the Department of Engineering Design. Her research interests cover industrial applications of color technology and pattern recognition.

Francesco Bianconi obtained a Laurea in Mechanical Engineering in 1997 from the University of Perugia, Italy, and received a Ph.D. in computer-aided design in 2000 from a consortium of italian universities. He is currently an Assistant Professor of Design Tools and Methods in Industrial Engineering at the Faculty of Engineering, University of Perugia. He has worked as visting researcher at the MIT and at the University of Vigo (Spain). His research interests cover: CAD/CAE, collaborative design and image processing. He is member of ACM and IEEE.

Paul F. Whelan (received his B.Eng. (Hons) degree from the National Institute for Higher Education Dublin, a M.Eng. degree from the University of Limerick, and his Ph.D. (Computer Science) from the University of Wales, Cardiff. During the period 1985-1990 he was employed by Industrial and Scientific Imaging Ltd and later Westinghouse (WESL), where he was involved in the research and development of industrial vision systems. He was appointed to the School of Electronic Engineering, Dublin City University (DCU) in 1990 and is currently a full Professor and holds a Personal Chair. Prof. Whelan set-up the Vision Systems Laboratory and its associated Vision Systems Group in 1990 and currently serves as its director. As well as a wide range of scientific publications, Prof. Whelan co-edited *Selected Papers on Industrial Machine Vision Systems* (1994), and was the co-author of *Intelligent Vision Systems for Industry* (1997) and *Machine Vision Algorithms in Java* (2000). His research interests include applied morphology, texture analysis, machine vision and medical imaging. He is a Senior Member of the IEEE, a Chartered Engineer and a member of the IEE and IAPR. He served on the IEE Irish centre committee (1999-2002) and is member of the governing board of the *International Association for Pattern Recognition (IAPR)* and the President of the *Irish Pattern Recognition and Classification Society*.